OFFPRINT

Barrier-mediated predator-prey dynamics

FABIAN JAN SCHWARZENDAHL and HARTMUT LÖWEN

Please visit the website
www.epljournal.org

epl

The Editorial Board invites you to submit your Letters to EPL

Choose EPL, and you'll be published alongside original, innovative Letters in all areas of physics. The broad scope of the journal means your work will be read by researchers in a variety of fields; from condensed matter, to statistical physics, plasma and fusion sciences, astrophysics, and more.

Not only that, but your work will be accessible immediately in over 3,300 institutions worldwide. And thanks to EPL's green open access policy you can make it available to everyone on your institutional repository after just 12 months.

Run by active scientists, for scientists

Your work will be read by a member of our active and international Editorial Board, led by Bart Van Tiggelen. Plus, any profits made by EPL go back into the societies that own it, meaning your work will support outreach, education, and innovation in physics worldwide.

**In 2020
Manuscripts published
received**

150

downloads on average

**In 2020
Perspective papers received**

350

downloads on average

**In 2020
"Editor's Choice"
articles received**

500

downloads on average

*We greatly appreciate
the efficient, professional
and rapid processing of our
paper by your team.*

Cong Lin
Shanghai University

Four good reasons to publish with EPL

1 **International reach** – more than 3,300 institutions have access to EPL globally, enabling your work to be read by your peers in more than 90 countries.

2 **Exceptional peer review** – your paper will be handled by one of the 60+ co-editors, who are experts in their fields. They oversee the entire peer-review process, from selection of the referees to making all final acceptance decisions.

3 **Fast publication –** you will receive a quick and efficient service; the median time from submission to acceptance is 78 days, with an additional 28 days from acceptance to online publication.

4 **Green and gold open access** – your Letter in EPL will be published on a green open access basis. If you are required to publish using gold open access, we also offer this service for a one-off author payment. The Article Processing Charge (APC) is currently €1,480.

Details on preparing, submitting and tracking the progress of your manuscript from submission to acceptance are available on the EPL submission website, **epletters.net**.

If you would like further information about our author service or EPL in general, please visit **epljournal.org** or e-mail us at **info@epljournal.org**.

EPL is published in partnership with:

European Physical Society   Società Italiana di Fisica   EDP Sciences   IOP Publishing

Barrier-mediated predator-prey dynamics

Fabian Jan Schwarzendahl(a) and Hartmut Löwen

Institut für Theoretische Physik II: Weiche Materie, Heinrich-Heine-Universität Düsseldorf
40225 Düsseldorf, Germany

Abstract – The survival chance of a prey chased by a predator depends not only on their relative speeds but importantly also on the local environment they have to face. Here, we propose a simple predator-prey model for a situation in which both the escaping prey and the chasing predator have to surmount an energetic barrier. Different barrier-assisted states of catching or final escaping are classified and suitable scaling laws separating these two states are derived. We discuss the effect of fluctuations on the catching times and determine states in which catching or escaping is more likely. We further identify trapping or escaping states which are determined by hydrodynamics and chemotactic interactions. Our results are of importance for both microbes and self-propelled unanimate microparticles following each other by non-reciprocal interactions in inhomogeneous landscapes.

Introduction. – The survival chances of animals depend crucially on their ability to find food and to escape from predators. In the macroscopic world, there is a plethora of examples where carnivores follow their prey trying to catch it but the prey tries to escape: wolf and deer, lion and wildebeest, shark and fish, etc. There are also microscopic examples such a droplets chasing each other [1], which will act as the central motivation for this study. Aside from stamina, the crucial parameter which determines the outcome of a chasing process are the two speeds v_1 and v_2 of the prey and the predator. Ideally, on the plane or in three-dimensional space, when the prey flees straight away from the predator, there will be catching for $v_1 < v_2$ and escaping for $v_1 > v_2$. This will be different, however, in an inhomogeneous landscape where the local speed depends on the details of the environment [2–4]. In particular, an obstacle which will be felt in a different manner by predator and prey will make the situation more complex such that the simple speed criterion will break down. Imagine a wolf following a deer when both come close to a river which can be jumped over by the deer but not by the wolf (the wolf has to slowly swim). Here the obstacle couples differently to predator and prey and this can decide after all the outcome of the chasing.

While a lot of previous work has modelled predator-prey coupling by coarse-grained density fields [5–9] or by explicit "particles" on a lattice [10–13], agent-based models with explicit interacting particles which follow each other on continuous individual trajectories [14–17] were much less considered. The latter models can particularly be designed for the mesoscopic world of phagocytes, predatory microbes moving in a fluid or other biological systems [18] in an overdamped way such that inertial effects are absent. Recently there has been a lot of activity in unanimate predator-prey systems designed by using synthetic colloidal particles which interact in a non-reciprocal way. Different realizations involve ion exchange resins building so-called "modular microswimmers" [19–23], moving droplets following each other [1,24], predator-prey–like entities for active colloidal molecules [25–29], pairs of dust particles in a complex plasma [30,31], and biomimetic active micromotor systems [32]. Even details of the particle perception can be programmed in synthetic colloidal model systems [33,34]. All of these systems naturally experience an inhomogeneous environment (such as confinement, external light intensity, etc.) when exhibiting predator-prey characteristics and are thus ideal test cases to study the effect of an energetic barrier on predator-prey dynamics.

In this letter we explore the effect of an energetic barrier on the escape dynamics of a predator-prey system within a simple model of two active particles in the presence of a parabolic potential energy barrier. Both the prey and the predator surmount the barrier but there are different coupling coefficients which make it easier for the prey respective to the predator to overcome the barrier. Here

---

(a)E-mail: Fabian.Schwarzendahl@hhu.de (corresponding author)

we propose a one-dimensional model which though simple is general enough to provide an ideal framework to classify different characteristic states for escape and catching in the presence of an obstacle. This model involves overdamped dynamics and is therefore likewise applicable for animate predator-prey systems as well as to unanimate self-propelled colloidal pairs with non-reciprocal interactions in the case they have to surmount an energetic barrier. The model is partially analytically soluble but flexibly extensible to more complicated couplings such as hydrodynamic interactions and chemotactic sensing.

We calculate the state diagram of escaping and catching situations in the parameter space and identify scaling laws for the catching time and catching position at the transition between catching and escaping. Next, fluctuations are included into the motion of both predator and prey. We compute the state diagram and we discuss the effect of noise strength. We then include hydrodynamic and chemotactic couplings between predator and prey and show their effect on the chasing outcome. We finally discuss the relevance of our results for both animate and unanimate particles following each other at low Reynolds number by non-reciprocal interactions.

Ideal predator-prey model. – We consider a one-dimensional model of predator and prey which are crossing a potential barrier. Figure 1(i) shows a schematic of prey $x_1(t)$ and predator $x_2(t)$ in the presence of their respective potential barrier $U(x_{1,2})$, where both are moving into the positive x-direction. Since we are motivated by microswimmers we are working in the low Reynolds number limit and assume the motion of predator and prey to be overdamped. The equations of motion for the position of the prey and the position of the predator are given by

$$\dot{x}_1 = v_1 + \alpha_1 x_1, \tag{1}$$
$$\dot{x}_2 = v_2 + \alpha_2 x_2, \tag{2}$$

where v_1, v_2 are the self-propulsion speeds, and α_1, α_2 are coupling constants to the respective potential barrier. Equations (1), (2) have the solutions

$$x_1(t) = \frac{1}{\alpha_1}((v_1 + \alpha_1 x_1(0))e^{\alpha_1 t} - v_1), \tag{3}$$
$$x_2(t) = \frac{1}{\alpha_2}((v_2 + \alpha_2 x_2(0))e^{\alpha_2 t} - v_2), \tag{4}$$

with initial conditions $x_{1,2}(0)$. We use $\tau = 1/\alpha_2$ as a natural unit of time and $\xi = v_2/\alpha_2$ as a natural length scale, which are the physical time and length scales related to the predator.

Single active particles similar to our equation (1) which are crossing a barrier have been studied theoretically in one-dimensional landscapes [35–39]. An experimentally realizeable system that is expected to have similar dynamics to our equations (1), (2) consists of two self-propelled droplets that chase each other such as in [1], and are confined into a one-dimensional microfluidic channel [24,40].
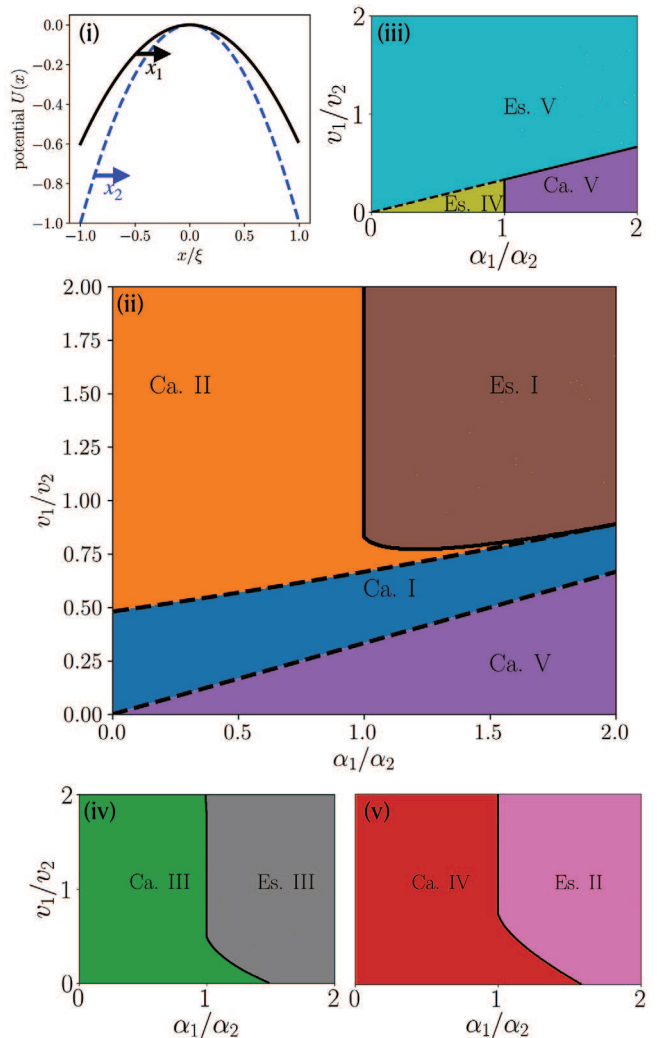

Fig. 1: Ideal predator-prey model. (i) Schematic of the prey (x_1) and predator (x_2) in the presence of a potential barrier $U(x)$ as a function of the reduced one-dimensional coordinate x/ξ. The black solid line shows the barrier of the prey and the blue dashed line shows the barrier of the predator. (ii) State diagram with initial conditions $x_1(0) = -\xi/3$ and $x_2(0) = -\xi/2$ showing catching and escaping regions for varying v_1/v_2 and α_1/α_2. For classification see table 1. (iii)–(v) State diagrams for different initial conditions. ((iii) $x_1(0) = -\xi/3$, $x_2(0) = -3\xi/2$; (iv) $x_1(0) = \xi/4$, $x_2(0) = -\xi/4$; (v) $x_1(0) = \xi/2$, $x_2(0) = \xi/4$).)

Additionally, the microfluidic channel has a physical barrier, that the droplets have to overcome, this physical barrier acts as potential barrier by means of the gravitational force. Here, the self-propulsion velocities can be tuned by the chemical compositions of the surrounding medium [41] and the coupling constants of the potential barrier can be tuned via the droplets' size. A barrier can also be realized by viscosity gradients in a surrounding fluid medium or external flow fields created in a microfluidic device [42].

In the following we want to distinguish the scenarios in which the predator can catch the prey and where it can

Table 1: Classification of catch (Ca.) and escape (Es.) cases, where x_1 is the prey and x_2 is the predator.

Case	Description	Initial conditions	Catching condition
Ca. I	Caught while summiting the barrier	$x_1(0) < 0,\ x_2(0) < x_1(0)$	$x^* > x_1(0)$
Ca. II	Caught after summiting the barrier	$x_1(0) < 0,\ x_2(0) < x_1(0)$	$x^* > 0$
Ca. III	Caught after prey summits	$x_1(0) > 0,\ x_2(0) \leq 0$	$x^* > 0$
Ca. IV	Caught descending barrier	$x_1(0) > 0,\ x_2(0) \geq 0$	$x^* > 0$
Ca. V	Caught descending barrier without summiting	$x_1(0) < 0,\ x_2(0) < x_1(0)$	$x^* < x_1(0)$
Es. I	Both are summiting the barrier	$x_1(0) < 0,\ x_2(0) < x_1(0)$	$x_1(\infty) = x_2(\infty) = \infty$
Es. II	Both descending in positive direction	$x_1(0) > 0,\ 0 < x_2(0) < x_1(0)$	$x_1(\infty) = x_2(\infty) = \infty$
Es. III	Both descending in opposite directions	$x_1(0) > 0,\ x_2(0) < 0$	$x_1(\infty) = \infty,\ x_2(\infty) = -\infty$
Es. IV	Both descending in negative direction	$x_1(0) < 0,\ x_2(0) < x_1(0)$	$x_1(\infty) = x_2(\infty) = -\infty$
Es. V	Only prey is summiting the barrier	$x_1(0) < 0,\ x_2(0) < 0$	$x_1(\infty) = \infty,\ x_2(\infty) = -\infty$

not. In order to determine catching we use the catching time t^* given by the condition

$$x_1(t^*) = x_2(t^*). \qquad (5)$$

Additionally, we use the catching position $x^* = x_{1,2}(t^*)$, which shows where the prey is caught. By considering the initial conditions and long-time limits of eqs. (3), (4) we can categorise five different catching cases and five different escaping cases which are summarized in table 1.

Figure 1(ii) shows the catching and escaping states for varying α_1/α_2 and v_1/v_2 with initial conditions $x_1(0) = -\xi/3 < 0$ and $x_2(0) = -\xi/2 < 0$ (here the condition in eq. (5) was solved numerically). We find three different catching states, where in Ca. I the prey is caught while summiting the barrier, in Ca. II the prey is caught after summiting the barrier and in Ca. V the prey is caught descending the barrier without summiting it. Furthermore, we find one escaping region (Es. I), where both are summiting the barrier.

We continue by analyzing the lines dividing the respective regions in fig. 1(ii). The line separating the regions Ca. I and Ca. II is determined by the fact that catching happens on top of the barrier, meaning that $x^* = 0$. In region Ca. I the prey can cross the barrier, while in Ca. V it cannot. Therefore, the line separating regions Ca. I and Ca. V can be determined from the long-time limits which gives $\frac{v_1}{v_2} = -x_1(0)\frac{\alpha_1}{\alpha_2}$.

The transition from the escape region Es. I and the catching regions was determined numerically. When we approach Es. I from below while increasing v_1/v_2, we find that at the transition line the catching time stays finite. For large α_1/α_2 this can be rationalized since we are going from Ca. I to Es. I. Here, the dividing line between catching and escaping approaches the line at which $x^* = 0$, meaning that catching happens before the barrier, or the prey escapes. Hence, the catching

time stays finite since $t(x^* = 0)$ is finite. This can also be seen when we solve eq. (5) for the special case $\alpha_1 = 2\alpha_2 = 2\alpha$ which stays finite (see Supplementary Material `Supplementarymaterial.pdf` (SM)).

On the other hand, as we approach the escape region from the left (from Ca. II), we find that catching time and position both diverge. To obtain an understanding of the scaling of the divergence, we approximate our solutions (eqs. (1), (2)) for barrier-dominated motion (see SM). We find that as we approach $\alpha_1 \to \alpha_2$, the catching time scales as $t^* \sim 1/(\alpha_1 - \alpha_2)$. Intuitively, for $\alpha_1 > \alpha_2$ the self-propulsion velocity of the predator is not sufficient anymore to catch the prey since the motion of both predator and prey is dominated by them descending the barrier. Similarly, as we come closer to from Ca. II to Es. I the catching dynamics becomes dominated by the potential barrier and the importance of the self-propulsion decreases. Here, it is interesting to see what happens at $\alpha_1 = \alpha_2 = \alpha$ when it is approached from below. This case can be solved exactly (see SM) where we find that t^* diverges as $\alpha \to \frac{v_2 - v_1}{x_1(0) - x_2(0)}$. Going along the line dividing the regions Ca. II and Es. I the point $\alpha_1 = \alpha_2 = \alpha$ is where the catching time starts to diverge and is thus consistent with the previous analysis.

Furthermore, we analysed the scaling of the relative distance, which to first order reads

$$x_1(t) - x_2(t) \approx A(t - t^*) + \dots. \qquad (6)$$

The prefactor A scales in the limit $\alpha_1 \to \alpha_2$ as $\ln A \sim 1/(\alpha_1 - \alpha_2)$ (see SM for details). Similar to the catching time, the relative position of predator and prey diverges, since their dynamics is dominated by them descending the potential barrier.

We continue by analyzing different initial conditions, that lead to other catching and escape scenarios.

Figure 1(iii) shows the state diagram for $x_1(0) = -\xi/3$ and $x_2(0) = -3\xi/2$, where we find the catching case Ca. V in which we have catching while both are descending the barrier without summiting and the escape cases Es. IV, where both descend into the negative direction, as well as the Es. V case where only the prey is able to summit the barrier. Here, the dividing lines between all respective regions were determined from the long-time limits of solutions in eqs. (3), (4).

Figure 1(iv) has initial conditions $x_1(0) = \xi/4$ and $x_2(0) = -\xi/4$ where we have one catching case Ca. III in which the prey is caught after summiting and escaping case Es. III, where predator and prey descend into opposite directions. Here, the dividing line between Ca. III and Es. III was determined numerically, however, the scaling arguments described above are still valid. Similarly, fig. 1(v) with initial condition $x_1(0) = \xi/2$ and $x_2(0) = \xi/4$ has one catching case Ca. IV, where the catching happens while descending the barrier and one escape scenario Es. II, where both are descending in the positive direction and the above scaling arguments still hold.

In the following we will extend our ideal predator-prey model (eqs. (1), (2)) to account for fluctuations, chemotactic and hydrodynamic interactions. Here, we will restrain ourselves to the initial conditions $x_1(0) = -\xi/3$ and $x_2(0) = -\xi/2$, since the essential phenomena of our model are captured within these conditions.

Predator-prey model with fluctuations. – We now extend our predator-prey model to account for fluctuations of both predator and prey. Our equations of motion are

$$\dot{x}_1 = v_1 + \alpha_1 x_1 + f_1, \qquad (7)$$
$$\dot{x}_2 = v_2 + \alpha_2 x_2 + f_2, \qquad (8)$$

where f_1 and f_2 are Gaussian random forces with $\langle f_i(t) \rangle = 0$ and $\langle f_i(t) f_i(t') \rangle = 2D\delta(t - t')$. Here, D is the noise strength and $\delta(*)$ is the Dirac-delta function. The random forces introduced here can stem from fluctuations of a surrounding fluid, however, they do not need to obey a fluctuation dissipation theorem since they can also be introduced by biological fluctuations (in the case of biological predator and prey). For fluctuating predator and prey the catching times and positions are now distributions by means of the random forces, f_1 and f_2 such that we need to use the mean catching time and the mean catching position to determine catching and escaping. By numerically integrating eqs. (7), (8) and taking mean values for catching time and position, we find the state diagram shown in fig. 2(i) where we used a fixed noise strength. The noisy behavior at the transition between the respective regions can be seen as an error bar on our numerical calculations. Similar to the situation without noise (fig. 1(ii)), we find three catching and one escape scenario, however, the relative size of the regions is changed by noise. Here, the fluctuations can help the predator to catch the prey.

To further investigate the effect of fluctuations we numerically solved eqs. (7), (8) and extracted the catching time distributions shown in fig. 2(ii) where we show a distribution for each catching or escaping case found in fig. 2(i). For the catching case Ca. I we find a broad distribution that has its maximum at $t^*/\tau \approx 0.1$ and then exhibits am shoulder towards higher catching times. In the case of Ca. II we find a bimodal distribution, with a maximum at $t^*/\tau \approx 3$ stemming from the deterministic dynamics and at $t^*/\tau \approx 0.1$ induced by fluctuations, which means that the prey is caught before summiting. In the case of Ca. V the distribution only has a single maximum and is centered around $t^*/\tau \approx 0.1$. For Es. I we find that fluctuations can cause catching for early times, however, we find a large peak at $t^*/\tau \approx 100$, which corresponds to escaping as this is our maximal simulation time. Note, that for all four cases we find a peak at $t^*/\tau \approx 100$, which should be categorised as escaping. For the catching cases Ca. I, Ca. II and Ca. V this is a "lucky" fluctuation-induced escaping of the prey.

Next, we test the dependence of our results on the strength of the noise D. Figure 2(iii) shows the catching time distribution for the case Ca. II ($\alpha_1/\alpha_2 = 0.5$, $v_1/v_2 = 1.5$) at different noise strength. For small noise strength ($D = 0.002\xi^2/\tau$) we find a sharp peak, and here fluctuations have minor effects. Going to higher values ($D = 0.02\xi^2/\tau$) the distribution becomes bimodal and then ($D = 0.2\xi^2/\tau$, $D = 2\xi^2/\tau$) spreads out to very low catching time values, with an approximate scaling $P(t^*) \sim (t^*)^{-3/2}$. For the latter, the catching process is dominated by fluctuations and the problem reduces to finding the first hitting time of a one-dimensional Brownian particle, which has the known scaling with an exponent of $-3/2$ [43], consistent with out finding. Again, for very large times ($t^*/\tau \approx 100$), all probability distributions show a peak, which signals escaping by fluctuations.

Continuing, we study the mean catching time for varying coupling ratio in fig. 2(iv). In the small noise limit, ($D = 0.002\xi^2/\tau$) the catching time diverges as we approach $\alpha_1 \to \alpha_2$, as also seen in the deterministic case ($D = 0$) (note that the plateau value for $D = 0.002\xi^2/\tau$ corresponds to the maximal simulation time). Going to higher noise strength the catching time is still enhanced for $\alpha_1 \to \alpha_2$, however, we find that the plateau value of mean catching time for $\alpha_1 > \alpha_2$ is decreased, representing the fact that fluctuations can lead to catching. Interestingly, for $D = 0.02\xi^2/\tau$ we find a small decay of the plateau value of the catching time for $(\alpha_1 - \alpha_2)/\alpha_2 \to 1$. This is due to the fact that for larger α_1 the prey needs a longer time to overcome the barrier and thus there is an enhancement of catching due to noise before crossing the barrier.

Chemotactic and hydrodynamic interactions. – To make a connection to microswimmers we study our predator-prey system in the presence of chemotactic and hydrodynamic interactions. Artificial droplet swimmers
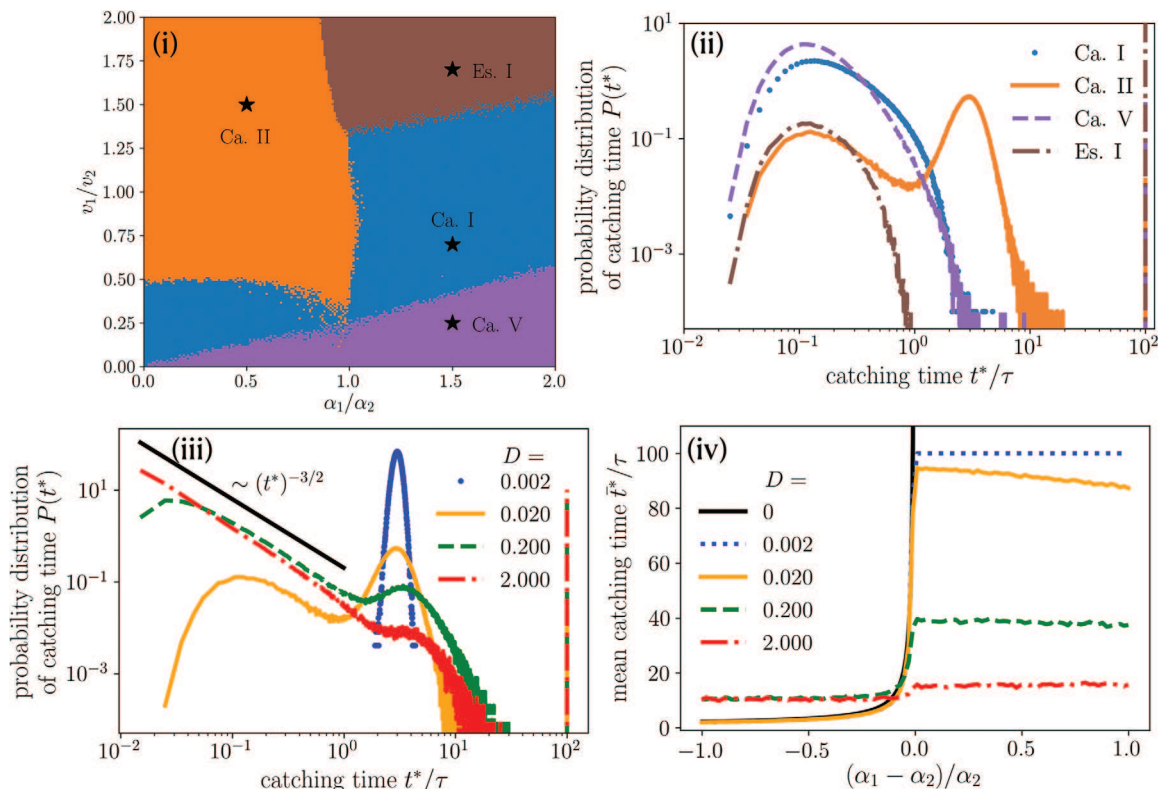
Fig. 2: Predator-prey model with fluctuations. (i) State diagram for different catching and escape cases for varying α_1/α_2 and v_1/v_2 (fixed $D = 0.02\xi^2/\tau$). The classification can be found in table 1. Stars show the values used for the representative catching time distributions in (ii). (ii) Representative catching time distribution for one example of each catching and escape case found in (i) (fixed $D = 0.02\xi^2/\tau$). (iii) Catching time distribution for different values of noise strength D. Black solid line shows a $P(t^*) \sim (t^*)^{-3/2}$ scaling. (iv) Mean catching time as a function of the relative coupling parameters for different noise strength D, at $v_1/v_2 = 1.75$.
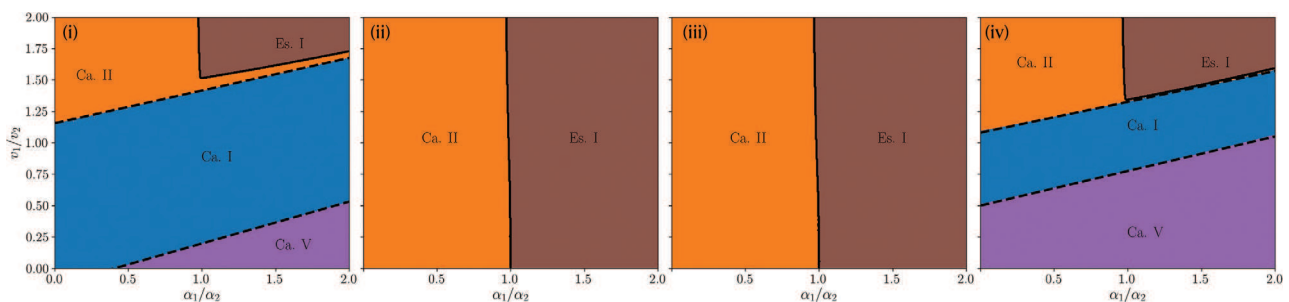

Fig. 3: State diagrams for models including chemotaxis and hydrodynamic interactions for varying v_1/v_2 and α_1/α_2. (i) Chemotaxis. (ii) Force monopole. (iii) Pusher-type swimmer. (iv) Puller-type swimmer. State classification is according to table 1.

such as in [1,24,40] interact via chemotaxis and hydrodynamic interactions have been shown to play an important role in suspensions of microswimmers [41,44–49].

We consider the situation where predator and prey interact through a chemical field. Both secrete a chemical which induces a force on the respective other swimmer and we neglect the effects of a confining channel (see SM for details [14,25,50]). We assume that the forces are proportional to the gradient of the chemical field which quickly relaxes to its stationary distribution. This gives rise to the

following equations of motion:

$$\dot{x}_1 = v_1 + \alpha_1 x_1 + A_1 \frac{1}{(x_1 - x_2)^2}, \tag{9}$$

$$\dot{x}_2 = v_2 + \alpha_2 x_2 + A_2 \frac{1}{(x_1 - x_2)^2}, \tag{10}$$

where A_1 and A_2 control the strength of chemoattraction or chemorepulsion.

Figure 3(i) shows the resulting state diagram for catching and escaping, where we used $A_1 = 0.001\xi^3/\tau$ and

$A_2 = 0.02\xi^3/\tau$. The catching and escaping regions that we find are the same as for the ideal model (see fig. 1(ii)), however, the relative sizes of the regions are changed by chemotactic interactions. Specifically, chemotaxis enhances the Ca. I case and reduces the extend of the escaping region Es. I, due to effective attraction between predator and prey.

Next, we consider the effect of a fluid surrounding predator and prey leading to hydrodynamic interactions. First, we investigate the situation in which both predator and prey act as a force monopole, leading us to the equations

$$\dot{x}_1 = v_1 + \alpha_1 x_1 + \frac{\beta}{4\pi\eta}\left(\alpha_2 \mathrm{sign}(x_1 - x_2) + \frac{v_2}{|x_1 - x_2|}\right),$$
$$(11)$$

$$\dot{x}_2 = v_2 + \alpha_2 x_2 + \frac{\beta}{4\pi\eta}\left(\alpha_1 \mathrm{sign}(x_2 - x_1) + \frac{v_1}{|x_1 - x_2|}\right),$$
$$(12)$$

where η is the fluids' viscosity, β is a parameter that depends on the geometric details of the swimmer and $\mathrm{sign}(*)$ is the sign function (for a derivation of the interactions see SM).

In fig. 3(ii) we show the resulting state diagram, where we only find two cases Ca. II and Es. I (here $\beta = 1/\tau$, $\eta = 1/(\tau\xi)$). The hydrodynamic interaction between predator and prey leads to an effective repulsion, such that it is easier for the prey to escape, enhancing the Es. I region. Similarly, the Ca. I and Ca. V regions vanish, since the predator and prey are repelled, making it necessary to first cross the border in order for predator and prey to come close enough for catching.

In a second step predator and prey induce a hydrodynamic flow field corresponding to a force dipole. Here, we use the equations

$$\dot{x}_1 = v_1 + \alpha_1 x_1 + \frac{\beta \mathrm{sign}(x_1 - x_2)}{4\pi\eta}\left(\alpha_2 + \frac{v_2\lambda}{(x_1 - x_2)^2}\right),$$
$$(13)$$

$$\dot{x}_2 = v_2 + \alpha_2 x_2 + \frac{\beta \mathrm{sign}(x_2 - x_1)}{4\pi\eta}\left(\alpha_1 + \frac{v_1\lambda}{(x_1 - x_2)^2}\right),$$
$$(14)$$

where the sign of λ decides whether we have puller- ($\lambda < 0$) or pusher-type ($\lambda > 0$) swimmers (for a derivation see SM).

The state diagram for pusher-type swimmers ($\lambda = 0.1\xi$, $\beta = 1/\tau$, $\eta = 1/(\tau\xi)$) is shown in fig. 3(iii). Here, the situation is similar to the force monopole. We find one catching region (Ca. II) and one escaping region (Es. I). The pusher-type hydrodynamic interactions introduce an effective repulsion between predator and prey, which gives rise to larger catching times and subsequently the enhancement of the Ca. II region. Similarly, the repulsion leads to the fact that catching happens less often and thus an increase of the Es. I region.

For puller-type swimmers ($\lambda = -0.1\xi$, $\beta = 1/\tau$, $\eta = 1/(\tau\xi)$) we find the state diagram shown in fig. 3(iv), which has three catching and one escape regions, similar to the ideal case (fig. 1(ii)). Here, the catching regions are enhanced since the puller-type hydrodynamic interactions give an effective attraction between predator and prey [51]. Interestingly, the Ca. V region is larger than in the ideal case, which shows that the attraction between predator and prey enhances catching before the barrier.

Conclusions. – In conclusion, we have introduced a one-dimensional predator-prey model in the presence of a potential barrier. We classified different catching and escaping states, calculated state diagrams displaying the occurrence of these states and determined scaling laws. We extended our model to account for fluctuations, computed a state diagram and showed that it qualitatively agrees with our ideal model. Here, the relative size of the catching regions is increased, since catching can be induced by fluctuations. We varied the noise strength and discussed the effect on catching times. Furthermore, we included chemotactic and hydrodynamic interactions. Chemotactic and puller-type swimmer interactions give a qualitatively similar state diagram as our ideal model, with an enhancement on catching states due to effective attractive interactions. On the other hand, pusher-type swimmers and hydrodynamic monopoles decrease the catching regions and enhance escaping, due to effective repulsion between predator and prey.

Our model makes testable predictions about the outcomes of predator-prey dynamics in the presence of a potential barrier in one dimension. A possible experimental realization of our model consists of two active droplets chasing each other [1] and encountering a physical barrier. Other realizations of barriers could be achieved by flow fields using microfluidic devices or by means of viscosity gradients. Furthermore, our model is relevant to microbial systems with predator-prey dynamics, that stem from chemotactic interactions.

In future work we aim to extend our model to two-dimensional landscapes [42,52,53], which might be realized by viscosity gradients [54–56] or external flow fields [57] and account for more realistic microswimmer models. Also, we will include inertial effects [58–61] to make a connection with macroscopic predator prey dynamics.

$$* * *$$

Data availability statement: The data that support the findings of this study are available upon reasonable request from the authors.

REFERENCES

[1] MEREDITH C. H., MOERMAN P. G., GROENEWOLD J., CHIU Y.-J., KEGEL W. K., VAN BLAADEREN A. and ZARZAR L. D., *Nat. Chem.*, **12** (2020) 1136.

[2] CUDDINGTON K. and YODZIS P., *Am. Nat.*, **160** (2002) 119.

[3] RAPOSO E. P., BARTUMEUS F., DA LUZ M. G., RIBEIRO-NETO P., SOUZA T. and VISWANATHAN G. M., *PLoS Comput. Biol.*, **7** (2011) e1002233.

[4] VOLPE G. and VOLPE G., *Proc. Natl. Acad. Sci. U.S.A.*, **114** (2017) 11350.

[5] CZIRÓK A., BEN-JACOB E., COHEN I. and VICSEK T., *Phys. Rev. E*, **54** (1996) 1791.

[6] PANG P. Y. and WANG M., *J. Differ. Equ.*, **200** (2004) 245.

[7] TSYGANOV M., BRINDLEY J., HOLDEN A. and BIKTASHEV V., *Phys. Rev. Lett.*, **91** (2003) 218102.

[8] KELLER E. F. and SEGEL L. A., *J. Theor. Biol.*, **30** (1971) 225.

[9] BORAAS M. E., SEALE D. B. and BOXHORN J. E., *Evol. Ecol.*, **12** (1998) 153.

[10] KAMIMURA A. and OHIRA T., *New J. Phys.*, **12** (2010) 053013.

[11] OSHANIN G., VASILYEV O., KRAPIVSKY P. and KLAFTER J., *Proc. Natl. Acad. Sci. U.S.A.*, **106** (2009) 13696.

[12] YANG S., JIANG S., JIANG L., LI G. and HAN Z., *New J. Phys.*, **16** (2014) 083006.

[13] SCHWARZL M., GODEC A., OSHANIN G. and METZLER R., *J. Phys. A: Math. Theor.*, **49** (2016) 225601.

[14] SENGUPTA A., KRUPPA T. and LÖWEN H., *Phys. Rev. E*, **83** (2011) 031914.

[15] ANGELANI L., *Phys. Rev. Lett.*, **109** (2012) 118104.

[16] JANOSOV M., VIRÁGH C., VÁSÁRHELYI G. and VICSEK T., *New J. Phys.*, **19** (2017) 053003.

[17] SURENDRAN A., PLANK M. J. and SIMPSON M. J., *Sci. Rep.*, **9** (2019) 14988.

[18] LI X., LIPOWSKY R. and KIERFELD J., *Biophys. J.*, **104** (2013) 666.

[19] IBELE M., MALLOUK T. E. and SEN A., *Angew. Chem., Int. Ed.*, **121** (2009) 3358.

[20] NIU R., PALBERG T., SPECK T. *et al.*, *Phys. Rev. Lett.*, **119** (2017) 028001.

[21] NIU R., FISCHER A., PALBERG T. and SPECK T., *ACS Nano*, **12** (2018) 10932.

[22] NIU R. and PALBERG T., *Soft Matter*, **14** (2018) 7554.

[23] LIEBCHEN B., NIU R., PALBERG T. and LÖWEN H., *Phys. Rev. E*, **98** (2018) 052610.

[24] JIN C., KRÜGER C. and MAASS C. C., *Proc. Natl. Acad. Sci. U.S.A.*, **114** (2017) 5089.

[25] SOTO R. and GOLESTANIAN R., *Phys. Rev. Lett.*, **112** (2014) 068301.

[26] LÖWEN H., *EPL*, **121** (2018) 58001.

[27] GONZALEZ S. and SOTO R., *New J. Phys.*, **21** (2019) 033041.

[28] SCHMIDT F., LIEBCHEN B., LÖWEN H. and VOLPE G., *J. Chem. Phys.*, **150** (2019) 094905.

[29] LIEBCHEN B. and LÖWEN H., *J. Chem. Phys.*, **150** (2019) 061102.

[30] IVLEV A. V., BARTNICK J., HEINEN M., DU C.-R., NOSENKO V. and LÖWEN H., *Phys. Rev. X*, **5** (2015) 011035.

[31] BARTNICK J., KAISER A., LÖWEN H. and IVLEV A. V., *J. Chem. Phys.*, **144** (2016) 224901.

[32] MOU F., LI X., XIE Q., ZHANG J., XIONG K., XU L. and GUAN J., *ACS Nano*, **14** (2019) 406.

[33] LAVERGNE F. A., WENDEHENNE H., BÄUERLE T. and BECHINGER C., *Science*, **364** (2019) 70.

[34] BÄUERLE T., LÖFFLER R. C. and BECHINGER C., *Nat. Commun.*, **11** (2020) 2547.

[35] CAPRINI L., MARINI BETTOLO MARCONI U., PUGLISI A. and VULPIANI A., *J. Chem. Phys.*, **150** (2019) 024902.

[36] GEISELER A., HÄNGGI P. and SCHMID G., *Eur. Phys. J. B*, **89** (2016) 175.

[37] SHARMA A., WITTMANN R. and BRADER J. M., *Phys. Rev. E*, **95** (2017) 012115.

[38] DHAR A., KUNDU A., MAJUMDAR S. N., SABHAPANDIT S. and SCHEHR G., *Phys. Rev. E*, **99** (2019) 032132.

[39] BLOSSEY R. and SCHIESSEL H., *J. Phys. A: Math. Theor.*, **52** (2019) 085601.

[40] DE BLOIS C., BERTIN V., SUDA S., ICHIKAWA M., REYSSAT M. and DAUCHOT O., arXiv:2103.09513 (2021).

[41] MAASS C. C., KRÜGER C., HERMINGHAUS S. and BAHR C., *Annu. Rev. Condens. Matter Phys.*, **7** (2016) 171.

[42] LIEBCHEN B. and LÖWEN H., *EPL*, **127** (2019) 34003.

[43] REDNER S., *A Guide to First-Passage Processes* (Cambridge University Press) 2001.

[44] SCHWARZENDAHL F. J. and MAZZA M. G., *J. Chem. Phys.*, **150** (2019) 184902.

[45] ZÖTTL A. and STARK H., *J. Phys.: Condens. Matter*, **28** (2016) 253001.

[46] THEERS M., WESTPHAL E., QI K., WINKLER R. G. and GOMPPER G., *Soft Matter*, **14** (2018) 8590.

[47] BECHINGER C., DI LEONARDO R., LÖWEN H., REICHHARDT C., VOLPE G. and VOLPE G., *Rev. Mod. Phys.*, **88** (2016) 045006.

[48] ELGETI J., WINKLER R. G. and GOMPPER G., *Rep. Prog. Phys.*, **78** (2015) 056601.

[49] DADDI-MOUSSA-IDER A., LÖWEN H. and LIEBCHEN B., *Commun. Phys.*, **4** (2021) 15.

[50] POHL O. and STARK H., *Phys. Rev. Lett.*, **112** (2014) 238303.

[51] GUZMÁN-LASTRA F., KAISER A. and LÖWEN H., *Nat. Commun.*, **7** (2016) 13519.

[52] YANG Y. and BEVAN M. A., *ACS Nano*, **12** (2018) 10712.

[53] ZIMMERMANN U., LÖWEN H., KREUTER C., ERBE A., LEIDERER P. and SMALLENBURG F., *Soft Matter*, **17** (2021) 516.

[54] COPPOLA S. and KANTSLER V., *Sci. Rep.*, **11** (2021) 399.

[55] DATT C. and ELFRING G. J., *Phys. Rev. Lett.*, **123** (2019) 158006.

[56] DANDEKAR R. and ARDEKANI A. M., *J. Fluid Mech.*, **895** (2020) R2.

[57] BERMAN S. A., BUGGELN J., BRANTLEY D. A., MITCHELL K. A. and SOLOMON T. H., *Phys. Rev. Fluids*, **6** (2021) L012501.

[58] SCHOLZ C., JAHANSHAHI S., LDOV A. and LÖWEN H., *Nat. Commun.*, **9** (2018) 5156.

[59] LÖWEN H., *J. Chem. Phys.*, **152** (2020) 040901.

[60] SPRENGER A. R., JAHANSHAHI S., IVLEV A. V. and LÖWEN H., *Phys. Rev. E*, **103** (2021) 042601 (arXiv:2101.01608 (2021)).

[61] CAPRINI L. and MARINI BETTOLO MARCONI U., *J. Chem. Phys.*, **154** (2021) 024902.